Divalent cations permeation in a Ca2+ non-conducting skeletal muscle dihydropyridine receptor mouse model

Romane Idoux, Clarisse Fuster, Vincent Jacquemond, Anamika Dayal, Manfred Grabner, Pierre Charnet, Bruno Allard

Divalent cations permeation in a non-Ca^{2+} conducting skeletal muscle dihydropyridine receptor mouse model

Romane Idoux[a], Clarisse Fuster[a], Vincent Jacquemond[a], Anamika Dayal[b], Manfred Grabner[b], Pierre Charnet[c], Bruno Allard[a]

a. Institut NeuroMyoGene, Université Lyon 1, UMR CNRS 5310 Inserm 1217, Faculté de Médecine et Pharmacie Rockefeller, 8 avenue Rockefeller, 69008 Lyon, France

b. Department of Medical Genetics, Molecular and Clinical Pharmacology, Division of Biochemical Pharmacology, Medical University of Innsbruck, Peter Mayr Strasse 1, A-6020, Innsbruck, Austria

c. Institut des Biomolécules Max Mousseron, UMR CNRS 5247, Université de Montpellier, 15 Avenue Charles Flahault, 34093 Montpellier, France

Corresponding author: Bruno Allard, bruno.allard@univ-lyon1.fr

Highlights

• The dihydropyridine receptor has a function of voltage-gated Ca^{2+} channel in muscle

• The N617D mutation in the α1 subunit confers non-Ca^{2+} conductivity to the channel

• Ba^{2+} and Mn^{2+} ions are found to permeate the mutant channel

• External Ca^{2+} strongly blocks Ba^{2+} currents through the mutant channel

• N617D mutation located outside the selectivity filter influences channel permeation

Abstract

In response to excitation of skeletal muscle fibers, trains of action potentials induce changes in the configuration of the dihydropyridine receptor (DHPR) anchored in the tubular membrane which opens the Ca^{2+} release channel in the sarcoplasmic reticulum membrane. The DHPR also functions as a voltage-gated Ca^{2+} channel that conducts L-type Ca^{2+} currents routinely recorded in mammalian muscle fibers, which role was debated for more than four decades. Recently, to allow a closer look into the role of DHPR Ca^{2+} influx in mammalian muscle, a knock-in (*ki*) mouse model (*nc*DHPR) carrying mutation N617D (adjacent to domain II selectivity filter Glu) in the DHPR α_1 subunit conferring non-Ca^{2+} conductivity to the channel was generated. In the present study, the Mn^{2+} quenching technique was initially intended to be used on voltage-clamped muscle fibers from this mouse to determine whether Ca^{2+} influx through a pathway distinct from DHPR may occur to compensate for the absence of DHPR Ca^{2+} influx. Surprisingly, while N617D DHPR muscle fibers of the *ki* mouse do not conduct Ca^{2+}, Mn^{2+} entry and subsequent quenching did occur because Mn^{2+} was able to permeate and produce L-type currents through N617D DHPR. N617D DHPR was also found to conduct Ba^{2+} and Ba^{2+} currents were strongly blocked by external Ca^{2+}. Ba^{2+} permeation was smaller, current kinetics slower and Ca^{2+} block more potent than in wild-type DHPR. These results indicate that residue 617 when replaced by the negatively charged residue Asp is suitably located at entrance of the pore to trap external Ca^{2+} impeding in this way permeation. Because Ba^{2+} binds with lower affinity to Asp, Ba^{2+} currents occur, but with reduced amplitudes as compared to Ba^{2+} currents through wild-type channels. We conclude that mutations located outside the selectivity filter influence channel permeation and possibly channel gating in a fully differentiated skeletal muscle environment.

Keywords: skeletal muscle fiber, voltage-gated Ca^{2+} channel, voltage clamp, dihydropyridine receptor, Cav1.1

1. Introduction

In skeletal muscle, contraction is triggered by an increase in the intracellular concentration of Ca^{2+}, a process which is under the tight control of the membrane potential of the cell. The voltage change produced by an action potential that spreads along the plasma membrane and in depth along the t-tubule membrane induces a change in the configuration of the dihydropyridine receptor (DHPR) which opens the Ca^{2+} release channel in the sarcoplasmic reticulum (SR) membrane [1-4]. This voltage-dependent control of SR Ca^{2+} channel opening and the release of Ca^{2+} that ensues is the primary role of the DHPR. The DHPR also functions as a voltage-gated Ca^{2+} channel that conducts a high threshold L-type Ca^{2+} current routinely recorded in mammalian voltage-clamped muscle fibers. Because Ca^{2+} influx through DHPRs is not required for Ca^{2+} to be released from the SR and contraction to be triggered [5], the occurrence and the functional role of Ca^{2+} influx through DHPR during physiological activation of the muscle cell have been recurrently questioned [6]. The technique of Mn^{2+} quenching of an intracellular Ca^{2+} indicator used to monitor Ca^{2+} influx during muscle activation has shown that Ca^{2+} does enter the muscle cell during a prolonged train of action potentials, producing an inward current of 0.3 A/F in mouse muscle [7]. Interestingly, in another vertebrate, the zebrafish, it was discovered that skeletal muscle DHPR exclusively operates as a voltage sensor controlling Ca^{2+} release and does not function as a Ca^{2+} channel, confirming that skeletal muscle could be functional without any DHPR Ca^{2+} influx [8].

The α_{1S} subunit is the main subunit of the DHPR that forms the voltage sensor and the pore of the channel. This subunit is composed of four homologous transmembrane domains (I to IV), each of which contains six membrane-spanning segments (S1 to S6) [9]. Four glutamate residues located at equivalent position in the S5-S6 loop of each domain constitutes the EEEE locus where most of the channel ion selectivity occurs. Sequence analysis of the α_{1S} subunit from zebrafish fast muscle fibers revealed the presence of an Asp residue at position 636 in domain II (position +3 relative to the conserved E of domain II involved in channel selectivity), conferring non-Ca^{2+} conductivity to the channel, since the replacement of an Asn by an Asp residue at position 617 in a rabbit α_{1S} subunit template led to a complete block of Ca^{2+} conductance [10]. A knock-in mouse model (*nc*DHPR) carrying the N617D mutation in the skeletal muscle DHPR was recently generated [11]. As expected, the L-type Ca^{2+} current was found to be eliminated in homozygous *nc*DHPR mice. These mice display SR Ca^{2+} release, locomotor activity and coordination, muscle strength, and susceptibility to fatigue, and fiber type specification comparable to wild-type controls suggesting that Ca^{2+} influx through the DHPR is irrelevant for muscle performance. The level of expression of

multiple key proteins involved in Ca^{2+} homeostasis was also found to be unchanged in these mice. However, possible occurrence of compensatory mechanisms for the absence of Ca^{2+} influx was not investigated at the functional level. The initial aim of the present study was to determine whether any Ca^{2+} influx may occur during muscle excitation to compensate for the absence of DHPR Ca^{2+} influx in mutant N617D DHPR mouse muscle. For this purpose, we used the Mn^{2+} quenching technique on voltage-clamped isolated skeletal muscle fibers from this mouse because of the very high resolution provided by this technique to detect Ca^{2+} entry [7, 12]. Surprisingly, while N617D DHPR expressing muscle fibers did not conduct Ca^{2+} ions in response to depolarization, we found that Mn^{2+} entry and subsequent quenching did occur because Mn^{2+} was able to permeate through the mutant N617D DHPR. The mutant N617D DHPR was also found to conduct Ba^{2+} ions and to be blocked by external Ca^{2+}. Finally, Ba^{2+} and Ca^{2+} permeation was investigated in wild-type DHPR to further understand how the N617D substitution conditions the difference in Ba^{2+} and Ca^{2+} permeation through the N617D DHPR.

2. Materials and methods

2.1. Preparation of mouse muscle fibers

All experiments were performed in accordance with the guidelines of the local animal ethics committee of the University Claude Bernard Lyon 1. Adult male C57BL10 and N617D DHPR mice [11] were killed by cervical dislocation before removal of *flexor digitorum brevis* muscles. Single fibers were isolated by a 50 minutes enzymatic treatment at 37° C using a Tyrode solution containing 2 mg/mL collagenase type I (Sigma).

2.2. Electrophysiology

Single fibers were voltage clamped using the silicone clamp technique as previously described [13]. The major part of a single fiber was electrically insulated with silicone grease and a micropipette was inserted into the fiber through the silicone layer to voltage clamp the portion of the fiber free of grease (50 to 100 μm length) using a patch-clamp amplifier (Bio-Logic RK-400, Claix, France) in whole-cell configuration. Command voltage pulse generation and data acquisition were done using the pClamp10 software (Axon Instruments Inc., USA) driving an A/D converter (Digidata 1400A, Axon Instruments Inc., USA). Analog compensation was systematically used to decrease the effective series resistance. Currents were acquired at a sampling frequency of 10 kHz. The holding potential was fixed at -80 mV throughout the study. Cell capacitance was determined by integration

of a current trace obtained with a 10-mV hyperpolarizing pulse from the holding potential and was used to calculate the density of currents (A/F). Leak currents were subtracted from all recordings using the same pulse preceding every test pulse supposing a linear evolution of leak current with depolarization. The voltage dependence of L-type current densities was fitted using the following equation: $I(V) = G_{max} (V - V_{rev}) / (1 + \exp ((V_{1/2} - V)/k))$, where I(V) is the mean density of the current measured, V the test pulse, G_{max} the maximum conductance, V_{rev} the apparent reversal potential, $V_{1/2}$ the half-activation voltage and k a steepness factor.

2.3. Mn^{2+} quenching experiments

Mn^{2+} influx was monitored by measuring the extinction of fura-2 fluorescence produced by Mn^{2+} binding to the indicator. Fura-2 fluorescence was measured at 520 nm upon excitation at the isosbestic wavelength. Images were captured with charge-coupled device camera (CoolSNAPEZ, Photometrics, Tucson, USA) at a frequency of 5 Hz during the voltage pulses and 0.5 Hz between pulses. Fluorescence values were expressed as percentage of the initial fluorescence recorded at the beginning of the experiment and corrected for background fluorescence measured next to each fiber. Prior to experiments, cells were dialyzed during 20 minutes with an internal pipette solution containing 100 µM fura-2 and 15 mM EGTA. At the beginning of each experiment, the isosbestic point was scanned by applying 1-s voltage steps to +20 mV to trigger SR Ca^{2+} release and changing the excitation wavelength around 360 nm by 1-nm step in the presence of an external solution containing Ca^{2+} until no change in fura-2 fluorescence was observed. Once the isosbestic point was found, 10 mM Mn^{2+} was substituted to 2.5 mM Ca^{2+} in the external solution.

2.4. Solutions

The external solution contained (in mM) 140 TEA-$MeSO_3$, 1 $MgCl_2$, 0.002 tetrodotoxine, 1 4-aminopyridine, 10 HEPES and either 10 $CaCl_2$, or 10 $MnCl_2$ or 10 $BaCl_2$, and the pH was adjusted to pH 7.2 with TEA-OH. To test the inhibition of the Ba^{2+} current by Ca^{2+}, the 10 mM $BaCl_2$ solution was supplemented with 0.1 or 1 mM $CaCl_2$. The intrapipette solution contained (in mM) 120 K-glutamate, 15 EGTA, 5 Na_2-ATP, 5 Na_2-phosphocreatine, 5.5 $MgCl_2$, 5 glucose, 5 HEPES adjusted to pH 7.2 with KOH. Experiments were carried out at room temperature.

2.5. Statistics

Fits were performed with Microcal Origin (Microcal Software Inc., Northampton, MA). Data are given as means ± s.e.m. and compared using two-tailed Student t-tests. Differences were considered significant when $P < 0.05$. Labels *, ** and *** indicate $P < 0.05$, $P < 0.005$ and $P < 0.0005$ respectively.

3. Results

3.1. Absence of voltage-activated L-type Ca^{2+} currents in N617D DHPR muscle fibers

The N617D DHPR mutation consists in the exchange of an Asn with an Asp residue at position 617 in the mouse skeletal muscle DHPR α_{1S} subunit (11). Asn 617 is located three amino acids downstream (+3) to the Glu residue at position 614 which belongs to a set of four conserved Glu residues (EEEE locus) in each of the P loop of the four domains that are critically involved in the pore selectivity filter (Fig. 1A). As shown in a previous study on N617D DHPR mice [11], we confirmed that depolarization never gave rise to any L-type Ca^{2+} currents in the presence of 10 mM external Ca^{2+} in all the fibers isolated from these mice (Fig. 1B, C).

3.2. Voltage-activated Mn^{2+} influx in N617D DHPR muscle fibers

We then investigated the possible existence of a parallel Ca^{2+} influx pathway activated by depolarization in these non-Ca^{2+} conducting cells using the Mn^{2+} quenching technique. Figure 2A shows that a depolarizing pulse to 0 mV induces a small but detectable quenching signal (lower traces) resulting from Mn^{2+} influx that further amplified and accelerated in response to pulses to +20 and +40 mV. Surprisingly, the quenching signals obtained at these voltage values were associated with inward membrane currents (upper traces) displaying kinetics reminiscent of those of L-type currents and which became more inward and faster until +40 mV depolarization. The inward current and the quenching signal were both reduced in response to a higher depolarization to +60 mV. Plotting the maximal peak amplitude of the quenching signal as a function of voltage yielded a relationship that closely resembled the one obtained in wild-type fibers when Mn^{2+} ions flow through L-type channels (Fig. 2B) (see 7).

3.3. Voltage-activated L-type Mn^{2+} and Ba^{2+} currents in N617D DHPR muscle fibers

These data likely suggest that the N617D DHPR mutation blocks Ca^{2+} permeation but allows Mn^{2+} ions to flow through the DHPR. A next series of experiments aimed at comparing the capacity of the N617D DHPR to produce voltage-activated L-type currents carrying Mn^{2+} and Ba^{2+} ions which

are routinely used as surrogate for Ca^{2+} ions through L-type Ca^{2+} channels. Figure 3A shows that Ba^{2+} currents did also permeate through N617D DHPR. The Ba^{2+} currents were of larger amplitude and their voltage-dependence and reversal potential were shifted toward negative voltages as compared to Mn^{2+} currents (Fig. 3B, table 1). Fitting a Boltzmann equation in every cell exposed to 10 mM Ba^{2+} indicated mean values of 127 ± 14 S/F, +50 ± 2 mV, +15 ± 3 mV and 4.4 ± 0.5 mV for G_{max}, V_{rev}, $V_{1/2}$ and k respectively. Mean values of G_{max},V_{rev}, $V_{1/2}$ and k in the presence of 10 mM Mn^{2+} were 64 ± 12 S/F, +59 ± 3 mV, +36 ± 4 mV and 5.3 ± 0.5 mV respectively, which, except for k, were significantly different from the respective values obtained in the presence of 10 mM Ba^{2+} (P was 0.0003, 0.0049, 0.016 and 0.37 for G_{max},V_{rev}, $V_{1/2}$ and k respectively). Ba^{2+} current activation was also slowed in average (Fig. 3C). Figure 4A shows that Ba^{2+} currents were blocked by the dihydropyridine compound nifedipine, confirming that the voltage-activated Ba^{2+} currents flowed through DHPR.

3.4. Blocking action of external Ca^{2+} on L-type Ba^{2+} currents in N617D DHPR muscle fibers

One possible explanation for the non-Ca^{2+} conductivity of N617D DHPR despite the ability of Ba^{2+} or Mn^{2+} to pass is that the channel permeability is reduced for the divalent cations, keeping a small permeability to Ba^{2+} or Mn^{2+}, but preventing the more affine Ca^{2+} ion to go through the channel. In this way, external Ca^{2+} ions may behave as blockers of the channel pore somehow like the well-known behavior of Cd^{2+} ions in the wild-type channel. The negatively charged Asp 617 is indeed located in the P loop of domain II at position +3 compared to the EEEE locus and -1 relative to a set of amino acids called Divalent Cation Selection (DCS) locus that has been shown to be involved in divalent cations selection of the channel [14]. In order to test this hypothesis, we evoked L-type Ba^{2+} currents in N617D DHPR fibers and added increasing concentrations of external Ca^{2+}. Figure 4B shows that the Ba^{2+} current was completely blocked by addition of 1 mM Ca^{2+} and was inhibited by 82 ± 4 % by addition of 100 µM Ca^{2+}. These results led us to conclude that external Ca^{2+} ions do act as channel blockers in the N617D DHPR.

3.5. Voltage-activated L-type currents in the presence of different external divalent cations in wild-type muscle fibers

Skeletal muscle DHPR is known to conduct Ba^{2+} and Ca^{2+} ions [15], but the possible behavior of Ca^{2+} ions as channel blockers when Ba^{2+} currents develop has never been investigated in skeletal muscle. Therefore, in a last series of experiments, we compared in wild-type fibers the amplitudes

and kinetics of L-type currents carried by Ca^{2+}, by Ba^{2+} and by Ba^{2+} with added Ca^{2+}. Figure 5 shows that G_{max} was found to be doubled in the presence of 10 mM external Ba^{2+} as compared to 10 mM Ca^{2+} (see also table 1). The kinetics of activation was also significantly faster. The other fitted parameters of the current-voltage relationships ($V_{1/2}$ and k) were not significantly changed, except V_{rev} which was significantly more positive in the presence of 10 mM Ca^{2+} than in the presence of 10 mM Ba^{2+} (see also table 1). Interestingly, addition of 1 mM Ca^{2+} to the 10 mM Ba^{2+} containing solution exerted a blocking action on L-type Ba^{2+} currents so that G_{max} and activation kinetics reached values close to those obtained with 10 mM external Ca^{2+} (table 1). The blocking action of external Ca^{2+} was clearly less pronounced in wild-type fibers since N617D DHPR Ba^{2+} currents were totally suppressed by addition of 1 mM external Ca^{2+} whereas G_{max} was only reduced by 47 ± 4 % in wild-type fibers. Finally, in the presence of 10 mM Ba^{2+}, G_{max} (320 ± 24 S/F) and V_{rev} (+66 ± 3 mV) were very significantly higher and more positive respectively for the wild-type DHPR as compared to the N617D DHPR (table 1) (P was < 0.0001 and 0.0003 for G_{max} and V_{rev} respectively), whereas $V_{1/2}$ and k were not significantly different, suggesting that channel voltage-dependence was little affected.

4. Discussion

The high resolution of the Mn^{2+} quenching technique led us to demonstrate that the N617D substitution in the α_1 subunit of the mouse skeletal muscle DHPR induced a complete block of voltage-gated L-type currents when Ca^{2+} was the charge carrier but allowed conduction of Mn^{2+} ions. Although the Mn^{2+} quenching technique was not helpful in this case to investigate a possible parallel voltage-activated Ca^{2+} entry pathway in N617D DHPR fibers, it revealed Mn^{2+} permeation through the mutant channel, and opened up in this way new opportunities to investigate structure-function relationship of divalent cations permeation through the skeletal muscle voltage-gated L-type Ca^{2+} channel in mature muscle fibers. The N617D DHPR was found to pass not only Mn^{2+} but also Ba^{2+} ions suggesting that the blocking action of divalent cations might be restricted to Ca^{2+} ions. Interestingly, the DHPR α_1 subunit of zebrafish fast muscle fibers, in which an aspartate residue constitutively replaces an asparagine residue at position 636, conducts neither Ba^{2+} nor Mn^{2+} ions [7, 10]. This difference in divalent cation permeation between the mouse muscle mutant N617D DHPR and the zebrafish muscle native N617D DHPR suggests that additional amino acids are involved in the total conductance blockade in zebrafish. The non-conserved serine at position -2 in

the first domain may constitute an interesting starting point to decipher the molecular basis of this difference between the mouse N617D channel and the zebrafish channel.

The potent blocking action of Ca^{2+} ions was firmly established here by demonstrating that Ba^{2+} currents through the N617D DHPR channel were completely inhibited in the presence of 1 mM Ca^{2+} added in the extracellular solution containing 10 mM Ba^{2+} while the same Ca^{2+} concentration inhibited Ba^{2+} currents by only 47 % in wild-type DHPR. Negatively charged Glu or Asp residues in EF hand motifs or in selectivity filters of Ca^{2+} channels provide the most common Ca^{2+} ligands in proteins [16, 17]. The affinity of these sites for Ba^{2+} ions is known to be lower, decreasing therefore the time of residency of Ba^{2+} within the pore. In this way, Ba^{2+} ions permeate Ca^{2+} channel more easily and activate less potently the EF hand containing Ca^{2+} binding protein calmodulin than Ca^{2+} ions do [16, 18]. The fact that the N617D mutation in the DHPR alters channel permeation and modifies slightly but not significantly the $V_{1/2}$ and the steepness of the voltage dependence indicates the alterations of the channel structure produced by this substitution are probably limited to the channel pore. One very likely interpretation of our results is that replacement of the neutral Asn residue at position 617 with Asp, just at the mouth of the channel pore, increases so strongly the affinity of the channel pore for Ca^{2+} that Ca^{2+} permeation is impeded. The mutated channel has also an increased affinity for Mn^{2+} and Ba^{2+} ions but that does not reach the point where ion flux is blocked. Consequently Mn^{2+} or Ba^{2+} currents still exist but are decreased by more than 80% (see 7) for Mn^{2+} currents through wild-type channels under comparable experimental conditions.

The structure of the rabbit Cav1.1, *i.e.* the α_1 subunit of the skeletal muscle DHPR, has been revealed by cryo-electron microscopy [19]. In the atomic model of the channel, the selectivity filter sequence containing the Glu residue in domain II is resolved. The asparagine residue at position 617 is located at the entrance of the channel pore, three amino acids downstream the glutamate residue involved in the selectivity filter in domain II and one amino acid before the DCS locus that has been shown to affect strongly cation divalent permeation [14]. Residue at position -1 relative to the E of selectivity filter of domain III has also been shown to perturb channel permeation [20]. The Cav1.1 model of Wu *et al.* [19] indicates that N617 points toward the selectivity filter of domain I and may engage non-covalent bonds with Gln287 and Glu292 of domain I (Fig. 6). In view of this, replacement of Asn 617 by Asp should produce a local rearrangement/modification of these interactions with a marked electrostatic influence that might modify the pore structure and hence the channel selectivity and permeability. Whether these changes affect the EEEE locus only or may propagate to the upper pore region and to the DCS locus is unknown. Whatever the mechanisms,

these changes are sufficient to create an inhibitory binding site for Ca^{2+} in the channel and a strong reduction in the channel permeability to Ba^{2+} and Mn^{2+}.

In the wild-type channel, Ca^{2+}, Mn^{2+}, and Ba^{2+} ions can all pass through the channel with the following relative L-type current amplitude sequence of $Ba^{2+} > Ca^{2+} > Mn^{2+}$ [7, 15, this study]. Single channel measurements of L-type currents in cardiac muscle showed that Ba^{2+} ions traverse the pore more rapidly than Ca^{2+} ions [21]. This difference of permeability results from a higher affinity of Ca^{2+} ions for binding sites in the selectivity filter within the pore which slows the travel of Ca^{2+} ions through the channel as compared to Ba^{2+} ions [16]. This tighter binding of Ca^{2+} ions within the pore also explains the higher selectivity of the channel for Ca^{2+} ions and the resulting significantly more positive reversal potential that we observed here for Ca^{2+} currents as compared for Ba^{2+} currents, as also described by Collet *et al.* [15]. Finally, the observed reduction in Ba^{2+} conductance induced by addition of 1 mM Ca^{2+} to the external Ba^{2+} containing solution confirmed that the higher affinity Ca^{2+} ions for intra-pore binding sites has a blocking effect on the flux of the lower affinity Ba^{2+} ion.

Unexpectedly, we observed throughout the study a close correlation between the conductance value of DHPR and the activation kinetics of the currents, *i.e.* the reduced Ba^{2+} currents in N617D DHPR displayed slower activation as compared to wild-type DHPR Ba^{2+} currents and Ca^{2+} currents, and Ba^{2+} currents with added Ca^{2+} activated more slowly than Ba^{2+} currents through wild-type DHPR. Such slowing of activation of voltage-gated L-type Ba^{2+} currents has been described in neurons in the presence of divalent metal cations exerting a blocking action on the channel [22]. In adult mouse skeletal muscle, Mn^{2+} currents flowing through L-type channels have also been found to activate more slowly than Ca^{2+} currents [7, 12]. The mechanisms involved in this phenomenon are not clearly established. However, because metal ions are able to interact with binding sites in the channel pore required for Ca^{2+} permeation [23], and/or in the present study possibly with Asp residue at position 617, one can speculate that such interactions with high affinity binding sites not only modify permeation but also the gating of the channel [22]. In agreement with this interpretation, Asp to Glu substitution in the selectivity filter of T-type Ca^{2+} channels was shown to slow activation of the Ca^{2+} current [24]. In addition, a recent work published by Abderemane-Ali *et al.* [25] demonstrated that the removal of a negative charge at position +1 relative to E in domain II of the Cav1.2 channel slightly affects selectivity but prevents Ca^{2+}-dependent inactivation, demonstrating that amino acid within the channel pore may affect current kinetics.

5. Conclusion

Very few data on Cav1.1 structure-function relationship are available in fully differentiated skeletal muscle fibers, except in the context of muscle diseases for which genetically engineered mouse models have been generated or mutated Cav1.1 have been transfected [26]. Also, it is always questionable if data obtained in cultured muscle cells or in heterologous expression systems, which, moreover, is only recently possible, are transferable to fully differentiated skeletal muscle fibers [27]. Here, we have shown that the N617D mutation in DHPR from fully differentiated skeletal muscle fibers induces profound alteration in the Ca^{2+} channel selectivity by reducing Ba^{2+} and Mn^{2+} and blocking Ca^{2+} permeation. These results indicate that divalent cation selection within the channel pore does not rely exclusively on the EEEE locus but is also influenced by amino acid located at entrance of the pore region of the Ca^{2+} channel of fully differentiated skeletal muscle.

Author contributions

R. Idoux and C. Fuster performed experiments and analyzed data. A. Dayal and M. Grabner provided the *nc*DHPR mouse model. P. Charnet performed molecular modeling. All authors made critical contributions to data interpretation and discussion and to manuscript preparation. B. Allard designed and performed experiments, analyzed data and wrote the paper.

Acknowledgments

This study was supported by the University Lyon 1, the Centre National de la Recherche Scientifique (CNRS), the Institut National de la Santé et de la Recherche Médicale (INSERM) and the Association Française contre les Myopathies (AFM-Téléthon, Alliance MyoNeurALP) and by the Austrian Science Fund (FWF) Grants P23229 to M.G. and P27392 to M.G. and A.D.). The authors declare that they have no competing interests.

References

1. Rios, E., G. Pizarro, Voltage sensor of excitation-contraction coupling in skeletal muscle, Physiol Rev. 71 (1991) 849-908.
2. Melzer, W., A. Herrmann-Frank, H.C. Lüttgau, The role of Ca^{2+} ions in excitation-contraction coupling of skeletal muscle fibres, Biochim Biophys Acta. 1241 (1994) 59-116.
3. Schneider, M.F, Control of calcium release in functioning skeletal muscle fibers, Annu Rev Physiol. 56 (1994) 463–484.

4. Allard, B, From excitation to intracellular Ca^{2+} movements in skeletal muscle: Basic aspects and related clinical disorders, Neuromuscul Disord. 28 (2018) 394-401.
5. Armstrong, C.M., F.M. Bezanilla, P. Horowicz, Twitches in the presence of ethylene glycol bis(-aminoethyl ether)-N,N'-tetracetic acid, Biochim Biophys Acta. 267 (1972) 605-608.
6. Bannister, R.A., K.G. Beam, Ca(V)1.1: The atypical prototypical voltage-gated Ca^{2+} channel, Biochim Biophys Acta. 1828 (2013) 1587-1597.
7. Robin, G., B. Allard, Voltage-gated Ca^{2+} influx through L-type channels contributes to sarcoplasmic reticulum Ca^{2+} loading in skeletal muscle, J Physiol. 593 (2015) 4781-4797.
8. Schredelseker, J., V. Di Biase, G.J. Obermair, E.T. Felder, B.E. Flucher, C. Franzini-Armstrong, M. Grabner, The β_{1a} subunit is essential for the assembly of dihydropyridine-receptor arrays in skeletal muscle. Proc Natl Acad Sci USA. 102 (2005) 17219-17224.
9. Catterall, W.A, Voltage-gated calcium channels, Cold Spring Harb Perspect Biol. 3 (2011) a003947.
10. Schredelseker, J., M. Shrivastav, A. Dayal, M. Grabner, Non-Ca^{2+}-conducting Ca^{2+} channels in fish skeletal muscle excitation-contraction coupling, Proc Natl Acad Sci USA. 107 (2010) 5658-5663.
11. Dayal, A., K. Schrötter, Y. Pan, K. Föhr, W. Melzer, M. Grabner, The Ca^{2+} influx through the mammalian skeletal muscle dihydropyridine receptor is irrelevant for muscle performance, Nat Commun. 8 (2017) 475.
12. Berbey, C., B. Allard, Electrically silent divalent cation entries in resting and active voltage-controlled muscle fibers, Biophys J. 96 (2009) 2648-2657.
13. Lefebvre, R., S. Pouvreau, C. Collet, B. Allard, V. Jacquemond, Whole-cell voltage clamp on skeletal muscle fibers with the silicone-clamp technique, Methods Mol Biol. 1183 (2014) 159-170.
14. Cens, T., M. Rousset, A. Kajava, P. Charnet, Molecular determinant for specific Ca/Ba selectivity profiles of low and high threshold Ca^{2+} channels, J Gen Physiol. 130 (2007) 415-425.
15. Collet, C., L. Csernoch, V. Jacquemond, Intramembrane charge movement and L-type calcium current in skeletal muscle fibers isolated from control and mdx mice, Biophys J. 84 (2003) 251–265.
16. Sather, W.A., E.W. McCleskey, Permeation and selectivity in calcium channels, Annu Rev Physiol. 65 (2003) 133-159.
17. Gifford, J.L., M.P. Walsh, H.J. Vogel, Structures and metal-ion-binding properties of the Ca^{2+}-binding helix-loop-helix EF-hand motifs, Biochem J. 405 (2007) 199-221.

18. Chao, S.H., Y. Suzuki, J.R. Zysk, W.Y. Cheung, Activation of calmodulin by various metal cations as a function of ionic radius, Mol Pharmacol. 26 (1984) 75–82.
19. Wu, J., Z. Yan, Z. Li, X. Qian, S. Lu, M. Dong, Q. Zhou, N. Yan, Structure of the voltage-gated calcium channel Cav1.1 at 3.6 Å resolution, Nature. 537 (2016) 191-196.
20. Williamson, A.V., W.A. Sather, Nonglutamate pore residues in ion selection and conduction in voltage-gated Ca^{2+} channels, Biophys J. 77 (1999) 2575-2589.
21. Hess, P., J.B. Lansman, R.W. Tsien, Calcium channel selectivity for divalent and monovalent cations. Voltage and concentration dependence of single channel current in ventricular heart cells, J Gen Physiol. 88 (1986) 293–319.
22. Castelli, L., F. Tanzi, V. Taglietti, J. Magistretti, Cu^{2+}, Co^{2+}, and Mn^{2+} modify the gating kinetics of high-voltage-activated Ca^{2+} channels in rat palaeocortical neurons, J Membr Biol. 195 (2003) 121–136.
23. Tang, L., T.M. Gamal El-Din, J. Payandeh, G.Q. Martinez, T.M. Heard, T. Scheuer, N. Zheng, W.A. Catterall, Structural basis for Ca^{2+} selectivity of a voltage-gated calcium channel. Nature. 505 (2014) 56-61.
24. Talavera, K., A. Janssens, N. Klugbauer, G. Droogmans, B. Nilius, Pore structure influences gating properties of the T-type Ca^{2+} channel α_{1G}, J Gen Physiol. 121 (2003) 529-540.
25. Abderemane-Ali F., F. Findeisen, N. D. Rossen, D.L. Minor Jr, A selectivity filter gate controls voltage-gated calcium channel calcium-dependent inactivation, Neuron. 101 (2019) 1134-1149.
26. Allard B, C. Fuster, When muscle Ca^{2+} channels carry monovalent cations through gating pores: insights into the pathophysiology of type 1 hypokalaemic periodic paralysis, J Physiol. 596 (2018) 2019-2027.
27. Olsson, K., A.J. Cheng, S. Alam, M. Al-Ameri, E. Rullman, H. Westerblad, J.T. Lanner, J.D. Bruton, T. Gustafsson, Intracellular Ca^{2+}-handling differs markedly between intact human muscle fibers and myotubes, Skelet Muscle. 5 (2015) 26. doi: 10.1186/s13395-015-0050-x.

Figures legends

Figure 1: Absence of voltage-activated L-type Ca^{2+} currents in N617D DHPR mouse muscle fibers. (A) Sequence alignment of the P loops of the wild-type α_{1S} subunit of DHPR with the typical EEEE locus in the four membrane domains (P1 to P4) that confers Ca^{2+} selectivity to the channel. In the N617D DHPR, the Asn residue at position 617 has been exchanged with an Asp residue (11). (B) Membrane currents (upper traces) recorded in response to depolarizing pulses applied to the

indicated voltages (lower panel) in the presence of 10 mM external Ca^{2+}. (C) Relationship between mean membrane current and membrane potential (n = 5).

Figure 2: Voltage-activated Mn^{2+} influx and membrane currents in N617D DHPR mouse muscle fibers. (A) Simultaneous recordings of membrane currents (upper traces) and changes in fura-2 fluorescence (lower traces) in the same fiber in response to depolarizing pulses of 10 s duration to the voltages indicated above the current traces. The lines below the fluorescence traces indicate the period during which the depolarizing pulses were applied. (B) Relationship between mean changes in fura-2 fluorescence and membrane potential (n = 5).

Figure 3: Voltage-activated L-type Mn^{2+} and Ba^{2+} currents in N617D DHPR mouse muscle fibers. (A) Membrane currents (upper traces) recorded in response to depolarizing pulses given to the indicated voltages (lower traces) in the presence of 10 mM external Mn^{2+} (left panel) and 10 mM external Ba^{2+} (right panel). (B) Relationships between membrane current and membrane potential in the presence of Mn^{2+} (open symbols, n = 4) and Ba^{2+} (closed symbols, n = 5). (C) Relationship between mean times to peak of voltage-activated L-type Ba^{2+} currents and membrane potential (closed symbols). The relationship obtained in wild-type fibers (open symbols) has been added to allow comparison (see Fig. 5).

Figure 4: Effect of nifedipine and external Ca^{2+} on voltage-activated L-type Ba^{2+} currents in N617D DHPR mouse muscle fibers. (A) Effect of 50 µM nifedipine on currents (upper trace) elicited by a voltage pulse delivered to +20 mV (lower trace) in the presence of 10 mM external Ba^{2+}. (B) Effect of increasing concentrations of external Ca^{2+} and washout on membrane currents (upper trace) elicited by a voltage pulse delivered to +30 mV (lower trace) in the presence of 10 mM external Ba^{2+}.

Figure 5: Voltage-activated L-type currents in the presence of different external divalent cations in wild-type mouse muscle fibers. (A) L-type currents (upper traces) in the presence of 10 mM Ba^{2+}, 10 mM Ca^{2+} and 10 mM Ba^{2+} + 1 mM Ca^{2+} in response to the indicated depolarizing pulses (lower traces). (B) Corresponding relationships between membrane current and membrane potential in the 3 ionic conditions (n = 12 for open symbols, n = 15 for black symbols and n = 11 for grey symbols). (C) Means of the fitting parameters of current-voltage relationships obtained in each fiber in the 3

ionic conditions. (D) Relationship between mean times to peak of voltage-activated L-type currents and membrane potential in the 3 ionic conditions.

Figure 6: N617 interactions with amino acids structuring the pore domain of Cav1.1. (A) Side view of cryo-electron microscopy structure of the pore domain around the amino acid N617 (pdb acc. Nb. 6BYO (19)). Only domains I and II are shown for clarity. The glutamate of domain I belonging to the selectivity filter (E292) and the glutamine of the same domain (Q287) are also labeled with the corresponding distances to H and O of N617. Amino acids facing the pore of domains I and II are shown in red and pink respectively (illustrated by using the PyMOL software). (B) Enlarged view of the non-covalent (H-bond and hydrophobic) interactions between N617 and neighboring amino acids. Only amino acids engaged in these interactions are shown (as determined by the Jmol software). E614 belonging to the selectivity filter of domain II is not in direct interaction with N617 and is therefore not represented in this view. Replacement of N617 by D is suspected to affect these interactions and thus structure of the pore and permeation.

Table 1: Mean maximal amplitude and V_{rev} of L-type currents in the presence of different external divalent cations in N617D DHPR and wild-type fibers.

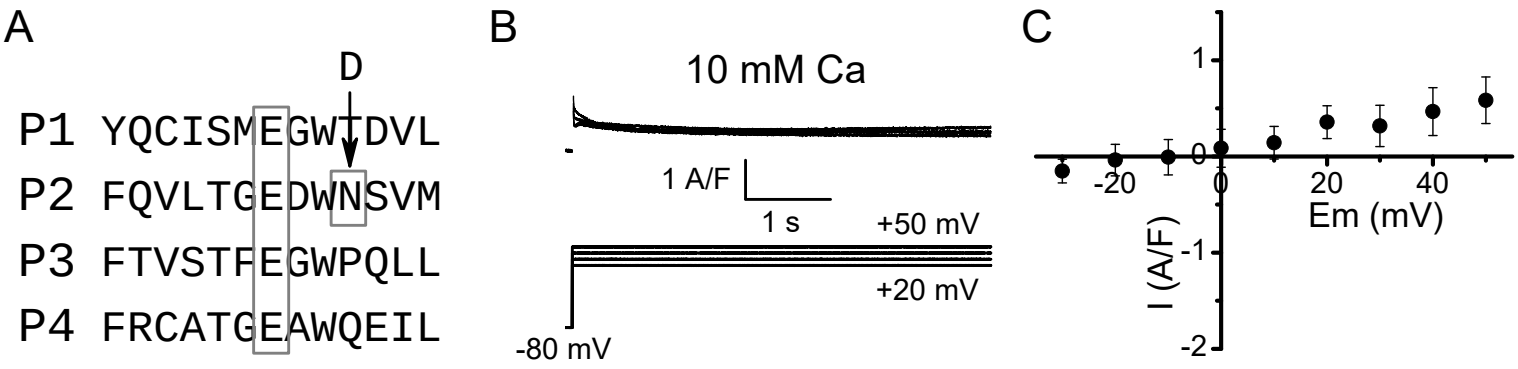
A
D
P1 YQCISMEGWTDVL
P2 FQVLTGEDWNSVM
P3 FTVSTFEGWPQLL
P4 FRCATGEAWQEIL
B
10 mM Ca
1 A/F
1 s
+50 mV
+20 mV
-80 mV
C
1
0
-1
-2
-20
0
20
40
Em (mV)
I (A/F)

Figure 1

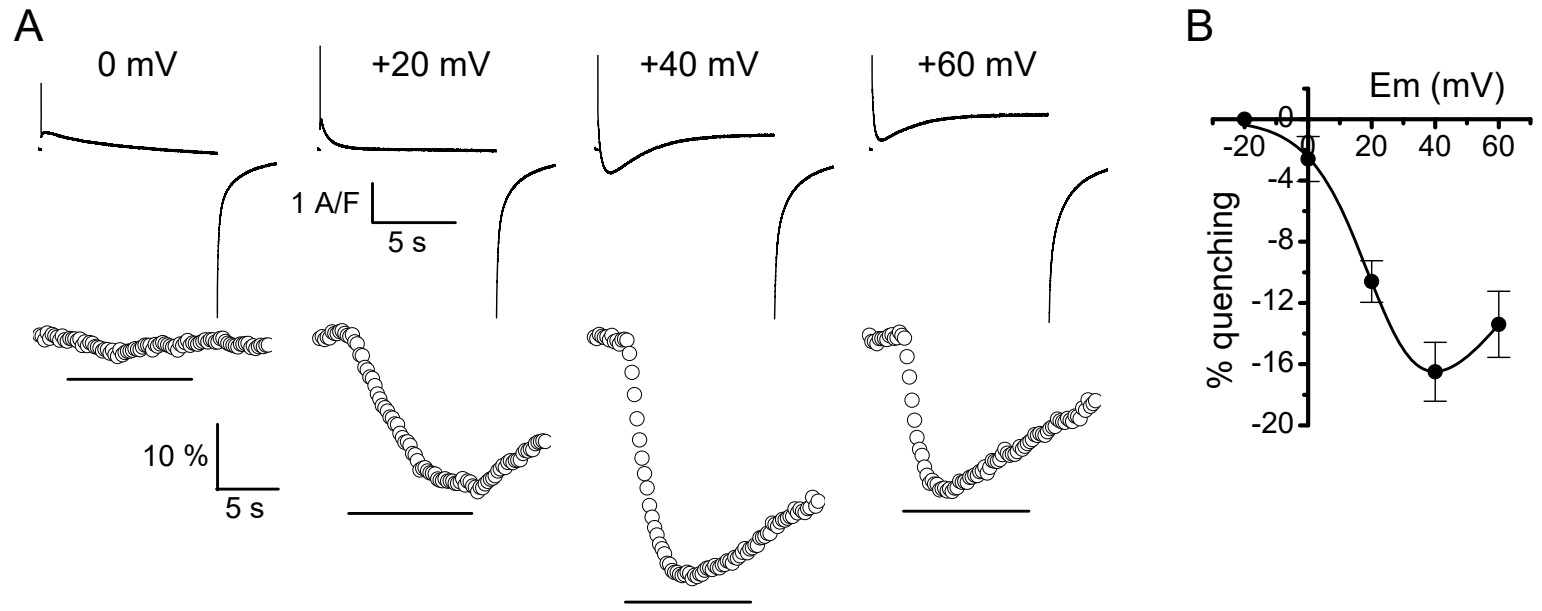
A
0 mV
+20 mV
+40 mV
+60 mV
1 A/F
5 s
10 %
5 s
B
Em (mV)
0
-20
0
20
40
60
-4
-8
-12
-16
-20
% quenching

Figure 2

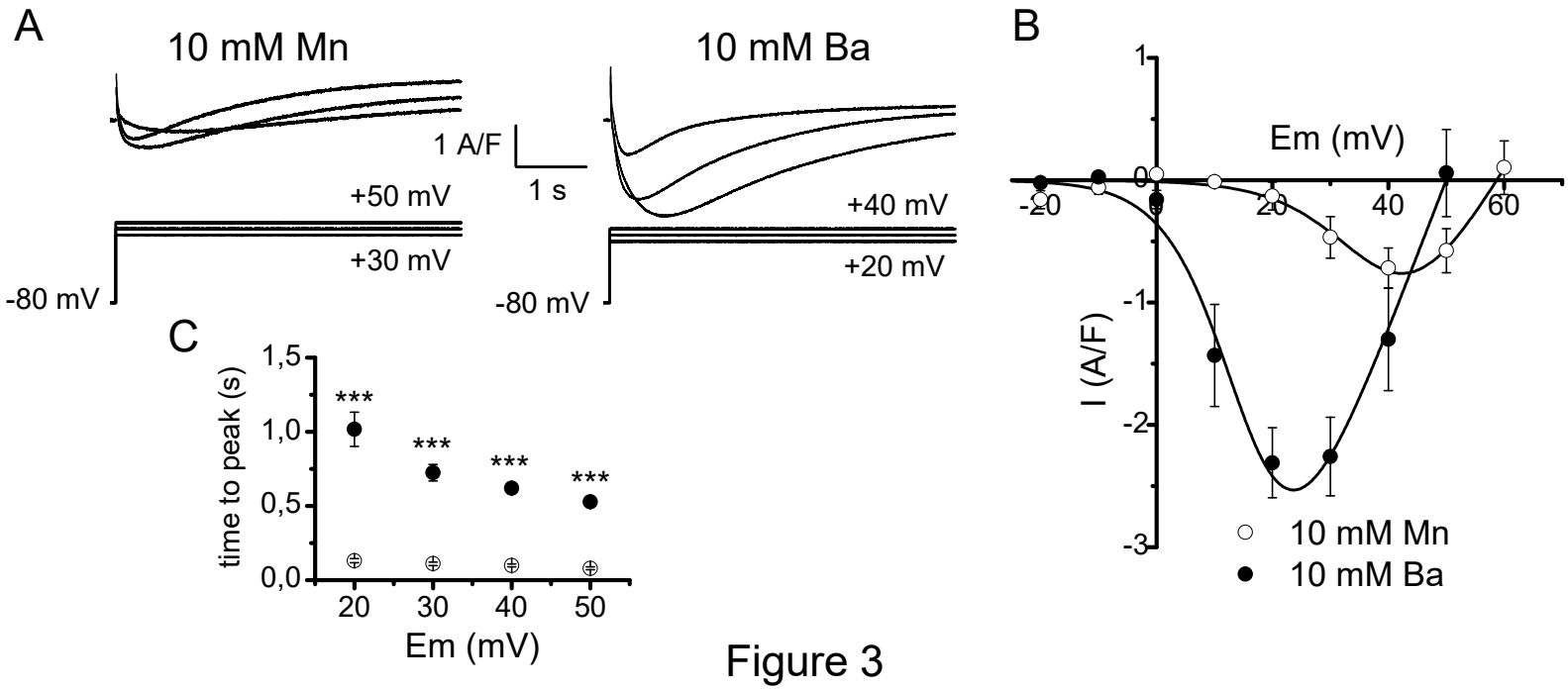
A
10 mM Mn
10 mM Ba
1 A/F
1 s
+50 mV
+30 mV
-80 mV
+40 mV
+20 mV
-80 mV
B
Em (mV)
I (A/F)
10 mM Mn
10 mM Ba
C
time to peak (s)
Em (mV)
***

Figure 3

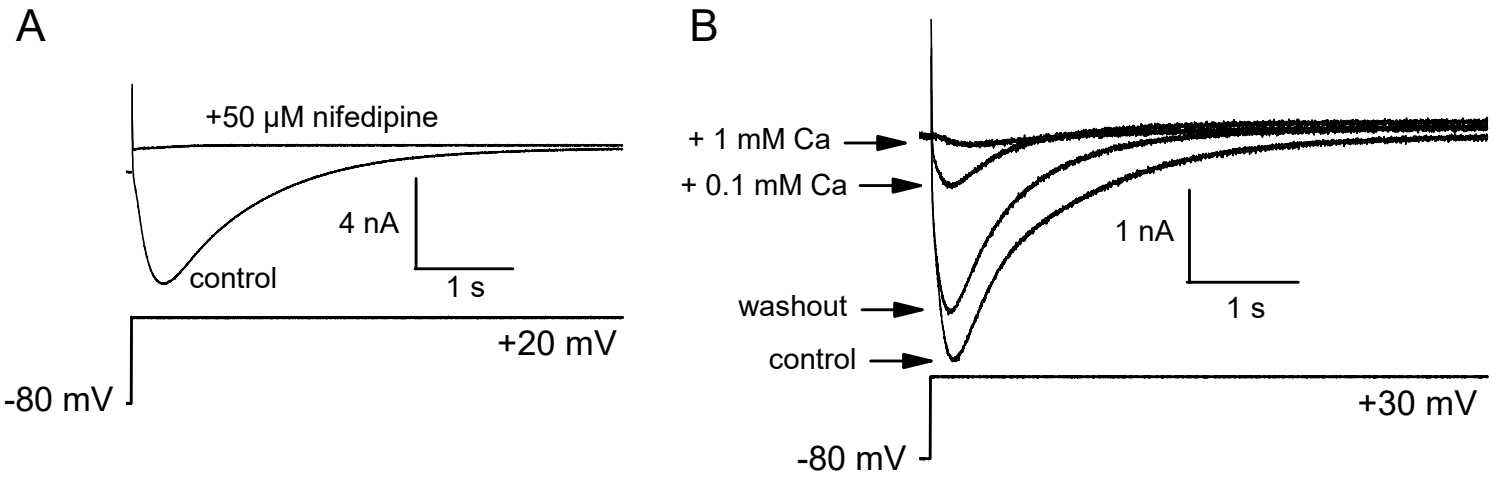
A
+50 µM nifedipine
4 nA
control
1 s
+20 mV
-80 mV
B
+ 1 mM Ca
+ 0.1 mM Ca
1 nA
1 s
washout
control
+30 mV
-80 mV

Figure 4

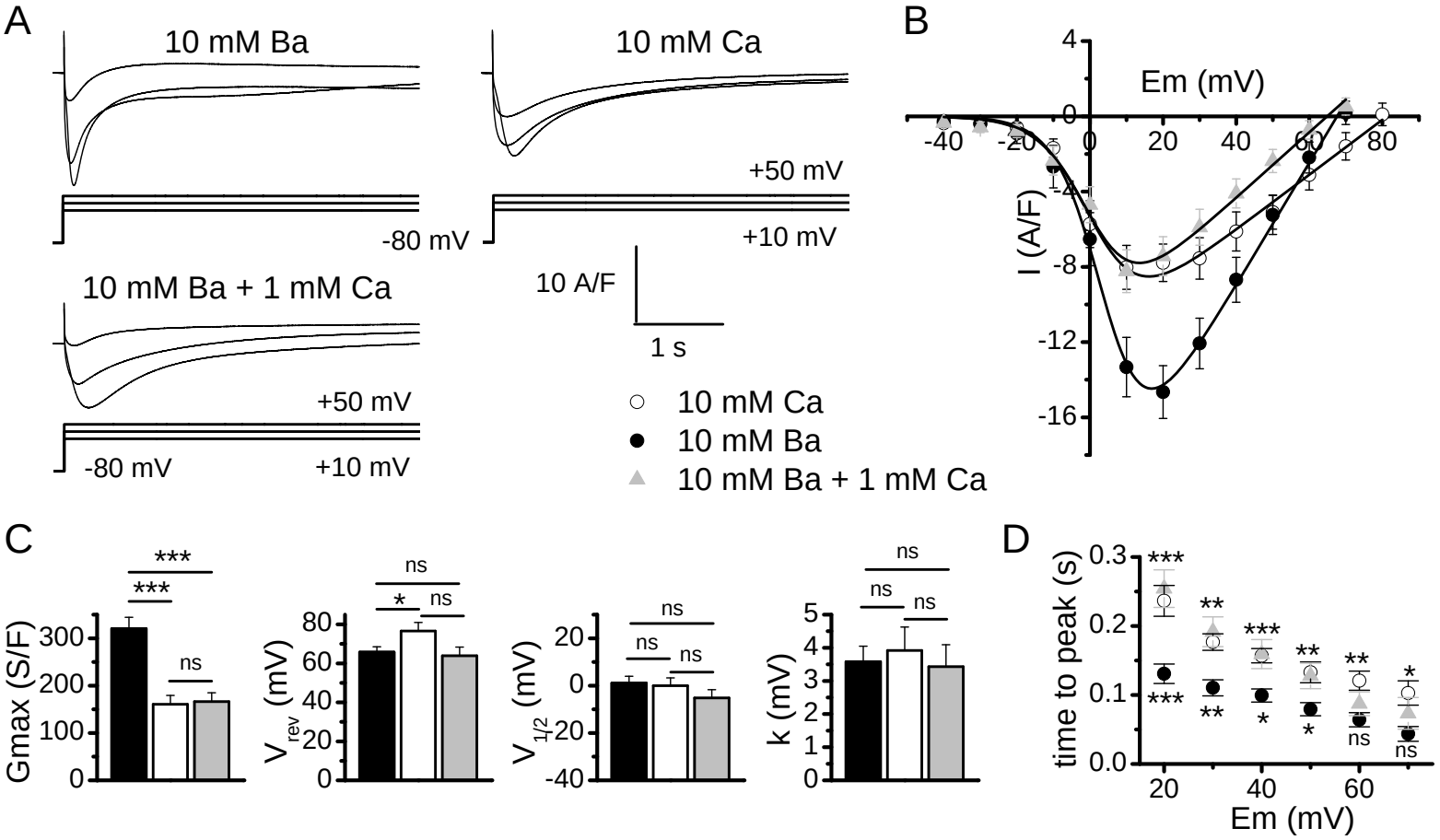
A
10 mM Ba
-80 mV
10 mM Ca
+50 mV
+10 mV
10 A/F
1 s
10 mM Ba + 1 mM Ca
+50 mV
-80 mV
+10 mV
B
Em (mV)
I (A/F)
10 mM Ca
10 mM Ba
10 mM Ba + 1 mM Ca

C
Gmax (S/F)
V_{rev} (mV)
$V_{1/2}$ (mV)
k (mV)
ns
D
time to peak (s)
Em (mV)

Figure 5

A

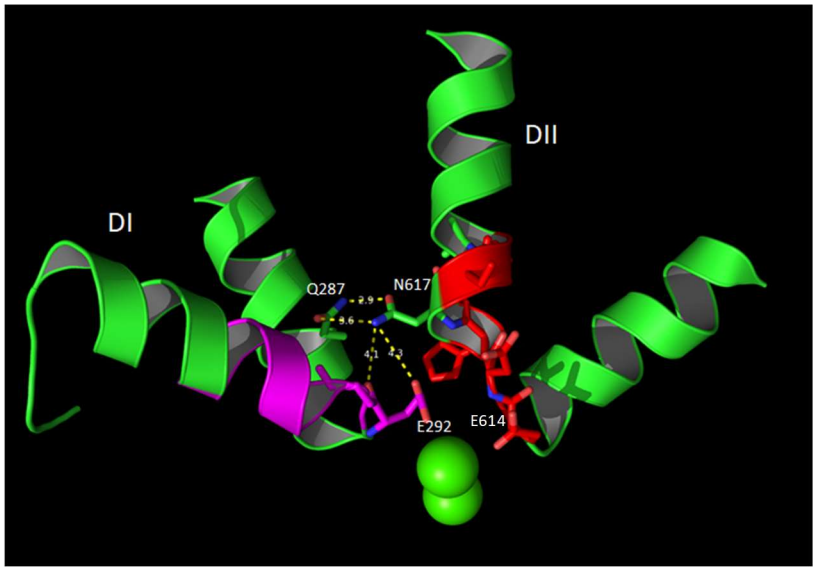
DII
DI
Q287
N617
E292
E614

B

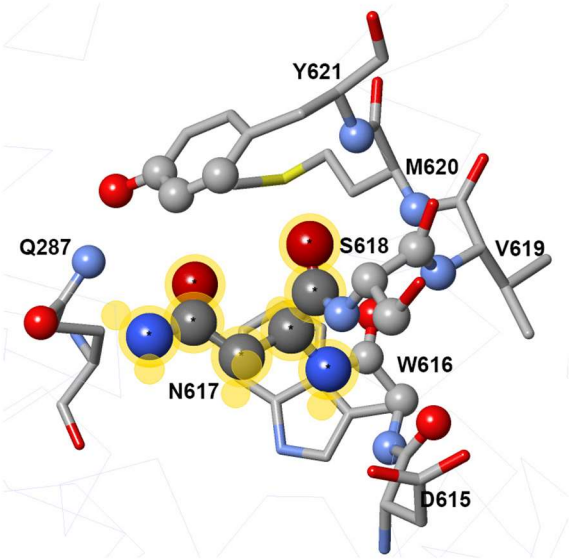
Y621
M620
Q287
S618
V619
W616
N617
D615

Figure 6

Table 1

	N617D DHPR muscle fibers	Wild-type muscle fibers
Mean maximal Ca^{2+} current amplitude (A/F)	0	-8 ± 1.2
Mean maximal Ba^{2+} current amplitude (A/F)	-2.3 ± 0.3	-14.6 ± 1.4
Mean maximal Mn^{2+} current amplitude (A/F)	-0.7 ± 0.2	-5.6 ± 0.6*
Mean maximal Ba^{2+} current amplitude with 1 mM added Ca^{2+} (A/F)	0	-8.2 ± 1.1
Mean Vrev of Ca^{2+} currents (mV)	/	+77 ± 4
Mean Vrev of Ba^{2+} currents (mV)	+50 ± 2	+66 ± 3
Mean Vrev of Mn^{2+} currents (mV)	+59 ± 3	+78 ± 3*
Mean Vrev of Ba^{2+} currents with 1 mM added Ca^{2+} (mV)	/	+64 ± 4

* data from (7)